Bulletin of the Seismological Society of America, Vol. 94, No. 2, pp. 394–409, April 2004

Stabilizing the Empirical Green Function Analysis: Development of the Projected Landweber Method

by Martin Vallée*

Abstract The empirical Green function approach is a very useful tool to study the seismic source properties when we are not able to model the propagation accurately. One of the problems of implementing the method, however, arises from the usual instability of the deconvolution inherent to the approach. Starting from the projected Landweber method introduced in seismology by Bertero *et al.* (1997), we propose to stabilize the process by taking into account physical constraints on the result of the deconvolution, which is in this case the relative source time function. Compared with Bertero *et al.*'s method, we add a new constraint that imposes that the area of the relative source time functions, which represents the seismic moment ratio, has to remain the same for all stations. We show how to take into account this important constraint in the framework of the projected Landweber method. Then, we illustrate with a synthetic example how this constraint is useful to model the earthquake kinematic process. Finally, we apply this technique to the very large 23 June 2001 Peru earthquake (M_w 8.4), for which we infer an along-trench rupture length of about 180 km. We image a high moment release 60-km-long zone 150 km away from the hypocenter.

Introduction

Knowledge of the seismic source requires modeling the propagation between the source and the receiver. Although simple teleseismic body waves (*P* and *SH* direct waves) can be precisely and deterministically estimated, most parts of the seismograms cannot, and that is why it is sometimes very helpful to use a smaller event to image the propagation between the source and the receiver. This approach was first proposed by Hartzell (1978). It was subsequently used and developed by Mueller (1985), Fukuyama and Irikura (1986), Mori and Frankel (1990), Ammon *et al.* (1993), Velasco *et al.* (1994), Courboulex *et al.* (1997a), and Ihmlé (1996). The idea is to deconvolve the mainshock from the smaller event, called the empirical Green function (EGF), to obtain a relative source time function (RSTF) at each considered station. The durations of each RSTF are then examined to retrieve some interesting properties regarding the extent and rupture velocity of the event. Information on the amplitude and shape of the RSTF is less easy to use, however, because it is more sensitive to the deconvolution process. We propose here a deconvolution method that takes into account various physical constraints of the RSTF to stabilize the deconvolution. The resulting RSTF is more reliable, and we are able to model it completely. The method is based on the projected Landweber method, introduced in seismology by Bertero *et al.* (1997), to which we have added an important constraint: the area of the RSTF, which represents the scalar moment of the earthquake, has to remain the same at all stations. We first outline the physical constraints on the RSTFs. Then, we detail how to compute the deconvolution. Finally, we illustrate, first with two synthetic examples and then with the 23 June 2001 Peru earthquake (M_w 8.4), the usefulness of the method.

*Present address: Osservatorio Vesuviano–Via Diocleziano, 328-80124 Napoli, Italia; vallee@ov.ingv.it.

Method

EGF Analysis

We recall here the theory of the EGF analysis to derive the physical constraints existing on the RSTFs. We start from the representation theorem (e.g., Aki and Richards, 1980) to express the spectral displacement $U_i(x,\omega)$ due to a discontinuity on a surface S represented by the moment density tensor m_{pq}:

$$U_i(\vec{x},\omega) = \int\int_S m_{pq}(\vec{\xi},\omega) G_{ip,q}(\vec{x},\vec{\xi},\omega) d^2\xi, \qquad (1)$$

where $G_{ip,q}$ denotes the spatial derivative of the Green function. We note $\vec{\xi}_0$ the hypocenter and we assume that the Green function G_{ip} is the same for all the points of the fault

except for a phase shift $\vec{k} \cdot (\vec{\xi} - \vec{\xi}_0)$ due to the varying distance between source and receiver (far-field approximation). We obtain

$$U_i(\vec{x},\omega) = -ik_q G_{ip}(\vec{x},\vec{\xi}_0,\omega) \iint_S m_{pq}(\vec{\xi},\omega) e^{-i\vec{k}\cdot(\vec{\xi}-\vec{\xi}_0)} d^2\xi. \quad (2)$$

We assume now that the earthquake has a constant mechanism, that is, m_{pq} can be written

$$m_{pq}(\vec{\xi},\omega) = \mathcal{M}_{pq} M f(\vec{\xi},\omega), \quad (3)$$

where

- $\mathcal{M}$ is a unit tensor independent of $\vec{\xi}$ and ω
- M is the scalar moment
- $f(\vec{\xi},t)$, the inverse Fourier transform of $f(\vec{\xi},\omega)$, is a causal, positive scalar function, monotonically increasing over $[0D]$, where D is the (unknown) duration of the source, and constant elsewhere

Thus the time derivative of f obeys the following properties:

$$\dot{f}(\vec{\xi},t) \begin{cases} \geq 0 & \text{if } 0 < t < D \\ = 0 & \text{elsewhere} \end{cases}. \quad (4)$$

Moreover, because of the use the scalar moment M, $\dot{f}$ has the property

$$\int_{-\infty}^{\infty} \iint_S \dot{f}(\vec{\xi},t) dt d^2\xi = 1. \quad (5)$$

For a large earthquake of moment M_1, we have

$$U_i^1(\vec{x},\omega) = -\mathcal{M}_{pq} M_1 ik_q G_{ip}(\vec{x},\vec{\xi}_0,\omega) \iint_S f(\vec{\xi},\omega) e^{-i\vec{k}\cdot(\vec{\xi}-\vec{\xi}_0)} d^2\xi. \quad (6)$$

If we can find, at the same location, a similar but smaller earthquake of scalar moment M_0, $f(\vec{\xi},\omega)$ can be approximated by

$$f(\vec{\xi},\omega) = \delta(\vec{\xi} - \vec{\xi}_0) TF(H(t)) = \frac{\delta(\vec{\xi} - \vec{\xi}_0)}{i\omega}, \quad (7)$$

where $TF(H(t))$ is the Fourier transform of the Heaviside function, which leads to

$$U_i^0(\vec{x},\omega) = -\mathcal{M}_{pq} \frac{M_0}{i\omega} ik_q G_{ip}(\vec{x},\vec{\xi}_0,\omega). \quad (8)$$

Therefore, by deconvolving equation (6) from equation (8), we obtain the RSTF, defined as F_θ in the equations:

$$F_\theta(\omega) = \frac{M_1}{M_0} i\omega \iint_S f(\vec{\xi},\omega) e^{-i\vec{k}\cdot(\vec{\xi}-\vec{\xi}_0)} d^2\xi. \quad (9)$$

We now write $\vec{k}$ as $\omega \cdot \vec{u}/v_\phi$, where v_ϕ, the phase velocity, and $\vec{u}$, the wave propagation direction, are assumed constant. This assumption compels us to study separately each wave type in the EGF analysis. We can then return to the time domain:

$$F_\theta(t) = \frac{M_1}{M_0} \iint_S \dot{f}(\vec{\xi},t - \vec{u} \cdot (\vec{\xi} - \vec{\xi}_0)/v_\phi) d^2\xi. \quad (10)$$

The use of surface waves theoretically adds some complexity to this method because they are dispersive, and therefore v_ϕ should be treated as a frequency-dependent parameter. This suggests that we should remain in the frequency domain of equation (9) and consider separately each frequency for a given phase velocity, as done by Ihmlé (1996) and Ihmlé and Ruegg (1997). According to global models, however, phase velocities do not vary significantly in the frequency range under consideration ($0.01 \text{ Hz} < f < 0.1 \text{ Hz}$), except for the very low frequencies. Moreover, the precise determination of these variations requires precise knowledge of the structure at the source, which is not always available. For these reasons, we shall assume, as did Ammon *et al.* (1993), that the use of an average phase velocity is a reasonable choice.

Equation (10) is interesting because it relates an observation to the spatiotemporal characteristics of the source $\dot{f}(\vec{\xi},t)$, without any complications due to the wave propagation between source and receiver. Even if we only know $\dot{f}(\vec{\xi},t)$ by its integral on the fault, the use of different stations and/or different waves (and therefore the modification of $\vec{u}$ and v_ϕ in equation 10) will allow us to retrieve some information about $\dot{f}(\vec{\xi},t)$ itself.

Because of the properties of the function $\dot{f}$, the RSTF is a positive, bounded-support function. The RSTF may be acausal, but we usually assume a propagating rupture, that is $\dot{f}(\vec{\xi},t) = 0$ for $t < \|\vec{\xi} - \vec{\xi}_0\|/v_r$, where the rupture velocity v_r is here assumed constant for clarity. The RSTF can then be acausal only if the rupture velocity is faster than the wave velocity. Even in this case, the RSTF is acausal only for stations where the propagation vector $\vec{u}$ satisfies

$$\|\vec{\xi} - \vec{\xi}_0\|/v_r - \vec{u} \cdot (\vec{\xi} - \vec{\xi}_0)/v_\phi < 0. \quad (11)$$

The duration of the RSTF will also depend on the position of the station, the phase, and the rupture velocity but will of course remain bounded. Using equation (5), we note a final property of the RSTF:

$$\int_{-\infty}^{\infty} F_\theta(t)dt = \frac{M_1}{M_0} \iint_S \int_{-\infty}^{\infty} \dot{f}(\vec{\xi},t - \vec{u} \cdot (\vec{\xi} - \vec{\xi}_0)/v_\phi)dtd^2\xi = \frac{M_1}{M_0}. \quad (12)$$

This integral value is independent of the stations or the wave type used in the deconvolutions and is equal to the relative moment between the mainshock and the EGF.

In the derivation of equation (10), we have specified the usual conditions on use of the EGF analysis. The three main restrictions are that (1) we must find a much smaller earthquake than the mainshock so that equation (7) is verified; (2) the mechanism and location must be similar—when there is some difference between both events, it is possible to correct for these effects (Ihmlé, 1996), but it adds some complexity to the procedure; and (3) the mainshock must have a constant mechanism so that the Green function may be assumed to be consistent over the whole source zone.

None of these conditions can be fully met, and we cannot avoid the errors introduced in the empirical determination of the Green function. The classical problem arises because these errors then appear in a division process (deconvolution) and can lead to unstable and erroneous results. We describe, in the next section, our approach to reducing this instability by accounting for these physical constraints on the RSTF.

Development of the Projected Landweber Method

The most commonly applied technique to reduce deconvolution instability is the water-level method. The idea is to perform a spectral division but to stabilize the denominator, that is, the spectrum of the EGF, by fixing a minimal value equal to this water level. By doing this, we avoid the inexact high amplitudes for some frequencies due to divisions by zero or very low values in the EGF spectrum. This method has been extensively used in EGF analysis (e.g., Velasco *et al.*, 1994; Courboulex *et al.*, 1997b; Schwartz, 1999). When this technique is used, we usually can identify some nonphysical features, that is, features not compatible with assumptions described in the previous section, in the obtained RSTFs:

1. There are some negative parts.
2. There is some acausal signal, that is, some signal arrives before the assumed beginning of the source time function (this is not theoretically impossible but can only happen when equation 11 is verified).
3. There is some signal after the assumed duration of the source time functions.
4. The area of the source time function, the relative moment between the mainshock and the EGF, is different from one station to another.

Incompatibilities (1) and (2) are sometimes addressed, for example by Courboulex (1997a), who considered the deconvolution as an inverse problem and could therefore reduce the parameter space to physical values only. However, by doing so, deconvolution becomes a complex process, not easy to use in a global analysis. Another approach was used by Velasco *et al.* (2000) based on an iterative deconvolution technique proposed by Kikuchi and Kanamori (1982). The idea is to look in the RSTFs for common contributions and then strip successively these contributions from the RSTFs until a complete explanation of the RSTFs is reached. The positivity constraint is simply imposed to the RSTFs.

Various methods can be implemented to solve a constrained inverse problem, such as constrained least-squares algorithms (Lawson and Hanson, 1974) or conjugate gradient methods. We have selected here the approach of Bertero *et al.* (1997), who have developed a simple method to address conditions 1, 2, and 3 based on the Landweber method. It was shown by Bertero *et al.* (1995) that the latter was slower but more accurate than conjugate gradient methods.

The main principles of the Landweber method are as follows: The problem is to identify the RSTF F_θ verifying

$$U^1 = U^0 * F_\theta, \quad (13)$$

where U^1 and U^0 are the mainshock and EGF waveform, respectively. Because of various unavoidable approximations, equation (13) generally does not have an exact solution, and we therefore seek an F_θ verifying

$$\|U^0 * F_\theta - U^1\| = \text{minimum}, \quad (14)$$

which is equivalent to solving

$$U^{0*} * U^{:0} * F_\theta = U^{0*} * U^1 \quad (15)$$

(e.g., Bertero, 1989), where U^{0*} is the adjoint operator of U^0. Because U^0 is simply a convolution operator, we have $U^{0*}(t) = U^0(-t) \forall t \in \mathcal{R}$. Equation (15) can thus be written

$$F_\theta = F_\theta + U^0(-t) * (U^1 - U^0 * F_\theta), \quad (16)$$

which leads to the following iterative process:

$$F_\theta^{(n+1)} = F_\theta^{(n)} + U^0(-t) * (U^1 - U^0 * F_\theta^{(n)}). \quad (17)$$

Practically, the process is convergent only if a relaxation parameter τ is added to equation (17):

$$F_\theta^{(n+1)} = F_\theta^{(n)} + \tau U^0(-t) * (U^1 - U^0 * F_\theta^{(n)}). \quad (18)$$

In the Landweber method, the relaxation parameter must satisfy $\tau \leq 2/(\sup_\omega |U^0(\omega)|)^2$ and is classically chosen to equal $1/(\sup_\omega |U^0(\omega)|)^2$. If used directly in the form of equation (18), this iterative process yields results similar to the water-level technique. However, a simple modification imposes some physical constraints on the RSTF. Suppose that we know that the RSTF belongs to some closed and convex set C. Then equation (18) can be modified as follows:

$$F_\theta^{(n+1)} = P_C(F_\theta^{(n)} + \tau U^0(-t) * (U^1 - U^0 * F_\theta^{(n)})), \quad (19)$$

where P_C denotes the metric projection on C. In the absence of noise, $F_\theta^{(n)}$ is shown to converge, but only weakly, toward the expected solution of

$$\|U^0 * F_\theta - U^1\| = \text{minimum}, F_\theta \in C. \quad (20)$$

Bertero *et al.* (1997) defined C as the set of nonnegative causal functions that are zero for $t > D$. But, in fact, we can be even more restrictive and let C be the set of nonnegative causal functions that are zero for $t > D$ and for which the integral over $[0D]$ is equal to M_1/M_0. We thus meet conditions 1, 2, 3, and 4. Figure 13 in Bertero *et al.*'s (1997) article shows how the equal moment constraint is important: when it is not used, the resulting moments can differ by as much as a factor of 2 depending on the stations. This discrepancy forbids completely the real modeling of the source time functions, and the only available information is the relative duration at each station.

It can be immediately verified that the newly defined set that we call *Cm* is closed and convex. We now must define the projection P_{Cm} itself in order to compute equation (19). Given a function h, it can be shown that $P_{Cm}(h)$ can be naturally computed, that is, we essentially add a proper, additive constant to h to derive $P_{Cm}(h)$ from h. The proof, omitted here, is based on the work of Youla and Webb (1982) and proceeds by showing, given a function $h \in L^2(\mathcal{R})$, that P_{Cm} verifies

$$I = \|h - P_{Cm}(h)\| = \int_{-\infty}^{\infty} (h(t) - P_{Cm}(h)(t))^2 dt = \text{minimum}. \quad (21)$$

We describe here only how this projection can be computed. Suppose that

$$\int_0^D P_+(h(t))dt = M', \quad (22)$$

where P_+ is defined by

$$P_+h(t) = \begin{cases} h(t) & \text{if } h(t)>0 \\ 0 & \text{elsewhere.} \end{cases} \quad (23)$$

We define the function g_k as

$$g_k(t) = h(t) + k\,\frac{M_1/M_0 - M'}{D}, \quad (24)$$

with k being a positive real number. We now consider

$$I_k = \int_0^D P_+(g_k(t))dt, \quad (25)$$

and by successive approximations, we define an estimation of k_0, the value of k having minimum magnitude such that

$$\text{sgn}(M_1/M_0 - I_k) = -\text{sgn}(M_1/M_0 - M'), \quad (26)$$

where sgn is the sign function [$\forall x \geq 0$, $\text{sgn}(x) = 1$; $\forall x < 0$, $\text{sgn}(x) = -1$]. P_{Cm} is then approximated by

$$P_{Cm}h(t) = \begin{cases} P_+\left(h(t) + k_0\,\dfrac{M' - M_1/M_0}{\alpha D}\right) & \text{if } t \in [0D] \\ 0 & \text{elsewhere.} \end{cases} \quad (27)$$

Given P_{Cm}, the computation procedure is again completely similar of the one of Bertero *et al.* (1997): we start from $F_\theta^{(0)} = 0$, compute equation (18) in the frequency domain, and come back to the time domain to use P_{Cm} as defined by equations (19) and (27). We then obtain $F_\theta^{(1)}$ and repeat the operation, transforming into the frequency domain to compute again equation (18) and so on. Lastly, we offer a few words about the stopping rules of the procedure. In the real case of noisy data, it has been numerically shown (Piana and Bertero, 1997) that scheme (19) is semiconvergent, that is, it approaches the solution before diverging again. However, the minimum seems very flat, and good results are obtained after a few hundred iterations.

Application to Synthetic Examples

Test of the Stability of the Method

To demonstrate the usefulness of this equal moment constraint, we investigate a classic, unilateral rupture on a straight fault. The rupture is assumed to occur on a 120-km-long, vertical, west–east–trending fault with a rupture velocity of 3 km/sec. Slip occurs instantaneously, and the slip distribution on the fault has a triangular shape, with the maximum occuring at the center of the fault (Fig. 1). The moment ratio between the mainshock and the EGF is chosen to be 1000. As the EGF, we choose a real signal, which is the Love-wave field of an M_w 5.8 earthquake that occurred on the North Anatolian fault on 13 September 1999 and was recorded at Incorporated Research Institutes for Seismology (IRIS) station MA2 (Fig. 2). Assuming a phase velocity of 4 km/sec, we can immediately compute the RSTFs at different azimuths from the event. We compute them in the three most interesting azimuths: the perpendicular direction (i.e., south or north), the directive direction (east), and the antidirective direction (west). In this simple case, the effect of the directivity is simply a compaction or an extension of the absolute source time function (i.e., the source time function in the perpendicular direction). Source time functions have a width of 40 sec in the perpendicular direction, 10 sec in the directive direction, and 70 sec in the antidirective direction (Fig. 1). By convolution of these three synthetic source time functions with the EGF signal, we obtain synthetic

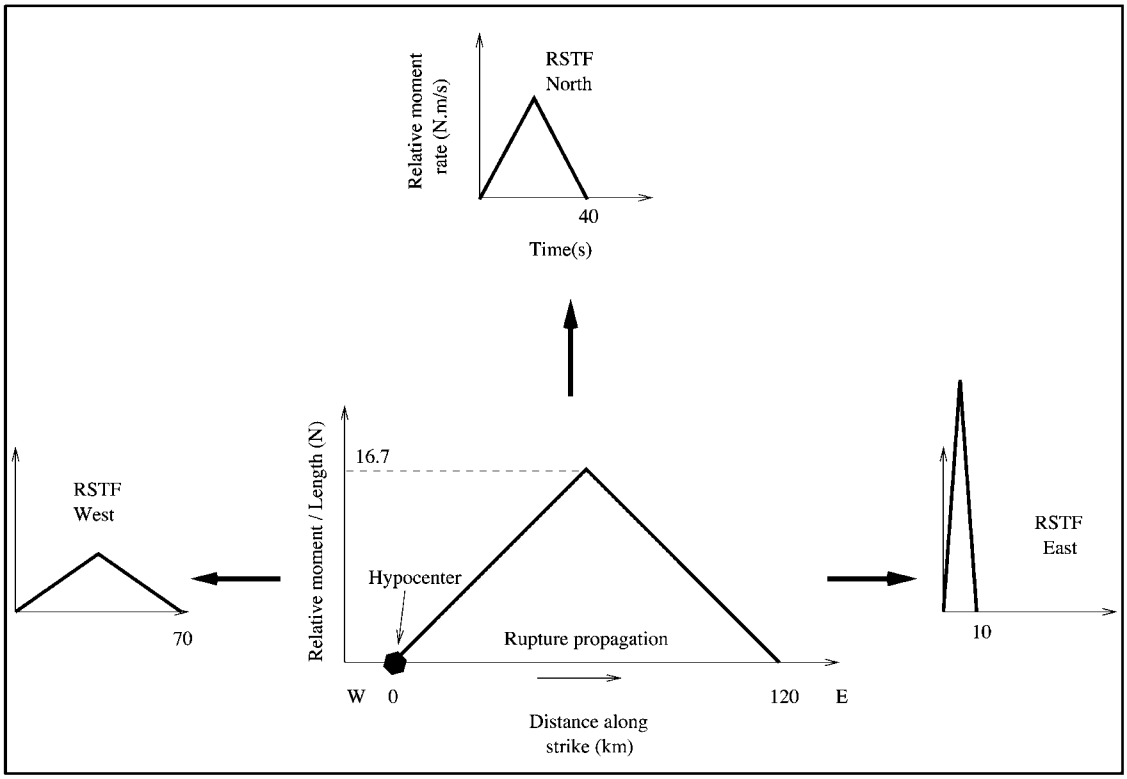

Figure 1. Source model used in the synthetic example: the hypocenter is located at the western extremity of the fault and rupture propagates toward the east at 3 km/sec. Slip occurs instantaneously at each point of the fault; thus the RSTFs observed at various azimuths all have the same triangular shape. The RSTFs are shown for the three considered azimuths, assuming a phase velocity equal to 4 km/sec.

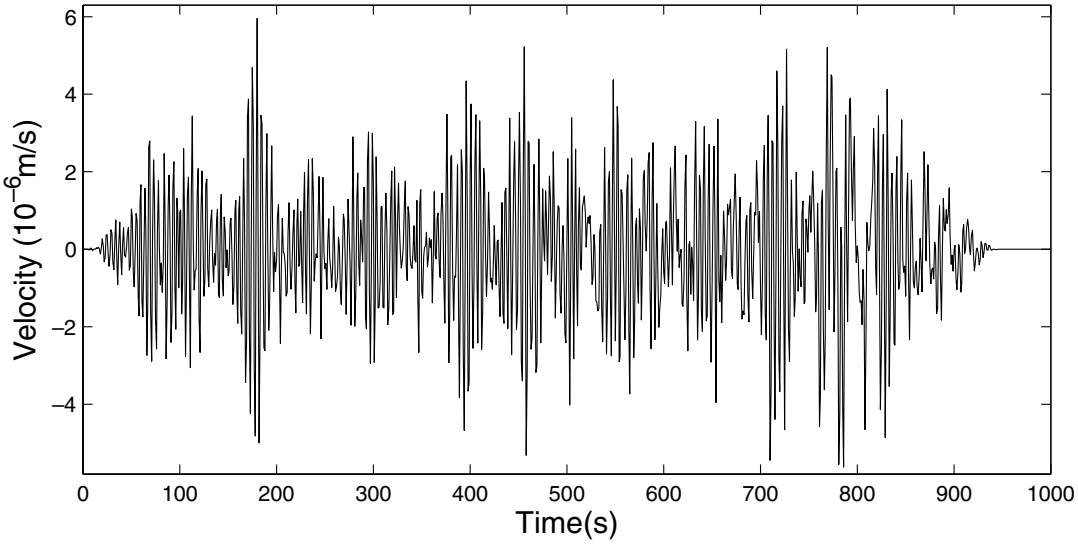

Figure 2. EGF used in the synthetic example. The EGF is a real earthquake ocurring on the North Anatolian fault, recorded at IRIS station MA2. This signal is convolved with the synthetic RSTFs to obtain the synthetic mainshocks. To test the deconvolution techniques, we have added some colored noise to this signal.

mainshock waveforms, presented in Figures 3d, 4d, and 5d. Let us now consider the inverse problem; the RSTFs and mainshock waveforms that we have obtained here will be referred to as the real waveforms.

We now examine how well we are able to retrieve the relative source time functions, given the mainshock and EGF signals, using different deconvolution techniques. To consider a more realistic case, we have corrupted the real EGF used to compute the synthetic waveforms: a colored noise, different for each station, having a similar spectral shape as the EGF, was added to the real EGF. The relative level of noise is about 25%. Deconvolution techniques are tested with these noisy EGFs. We use our version of the Landweber method, which takes into account not only causality, positivity, and finite duration of the RSTFs but also the fact that the moment ratio between the mainshock and EGF is 1000. We use 500 iterations of scheme (18), and we use the projected equation (19) only once in every 10 iterations. This is a way to accelerate the procedure (Piana and Bertero, 1997). We present in Figures 3(a–d), 4(a–d), and 5(a–d) for each of the three directions (a) the misfit between the real mainshocks and the reconstituted mainshock obtained by reconvolution of the RSTF with the EGF, as a function of the allowed duration of the RSTF—this misfit is a good indicator of the quality of the obtained deconvolution; (b) the evolution of the obtained seismic moment as a function of the allowed duration of the RSTF; (c) the preferred RSTF; and (d) a comparison between the real mainshock and the reconstituted mainshock for the preferred RSTF. We present in parallel the corresponding results with Bertero *et al.*'s (1997) technique, which takes into account only three physical constraints: causality, positivity, and finite duration. The preferred RSTFs are also compared (Figs. 3c, 4c, and 5c) with the RSTF obtained by the classical water-level method.

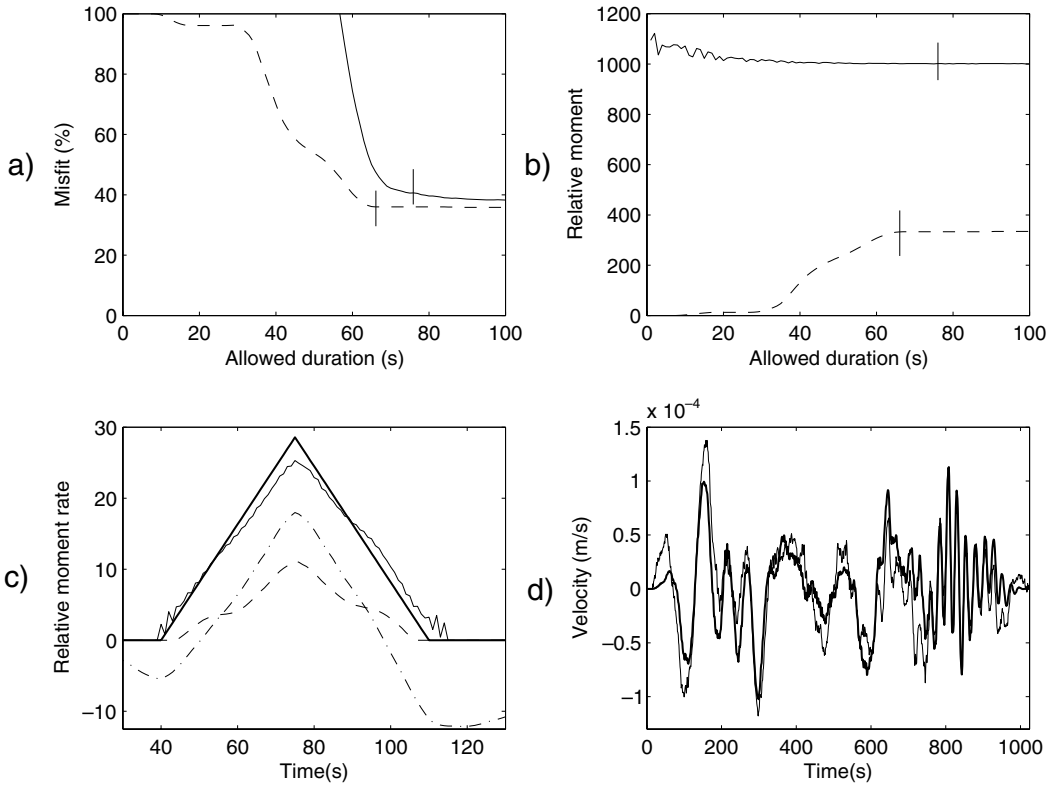

Figure 3. Results obtained in the antidirective direction for the three deconvolution techniques considered in the synthetic case: (1) constrained moment method, (2) Bertero *et al.*'s (1997) method, and (3) classical water-level method. Plain lines refer to technique 1, dashed lines to technique 2, and dash-dotted lines to technique 3. (a) For techniques 1 and 2, the misfit between the real mainshocks and the reconstituted mainshock obtained by reconvolution of the RSTF with the EGF, as a function of the allowed duration of the RSTF. The vertical ticks indicate the time after which there is no more improvement of the reconstituted mainshock. (b) For techniques 1 and 2, the evolution of the obtained seismic moment as a function of the allowed duration of the RSTF. (c) The preferred RSTF for techniques 1 and 2, as well as the RSTF obtained by technique 3. The preferred RSTFs are the RSTFs constrained to the durations indicated by the vertical ticks in (a) and (b). The thick line is the real RSTF. The origin time of the RSTFs is fixed at 40 sec. (d) A comparison between the real mainshock (thick line) and the reconstituted mainshock for the preferred RSTFs with technique 1 (thin line).

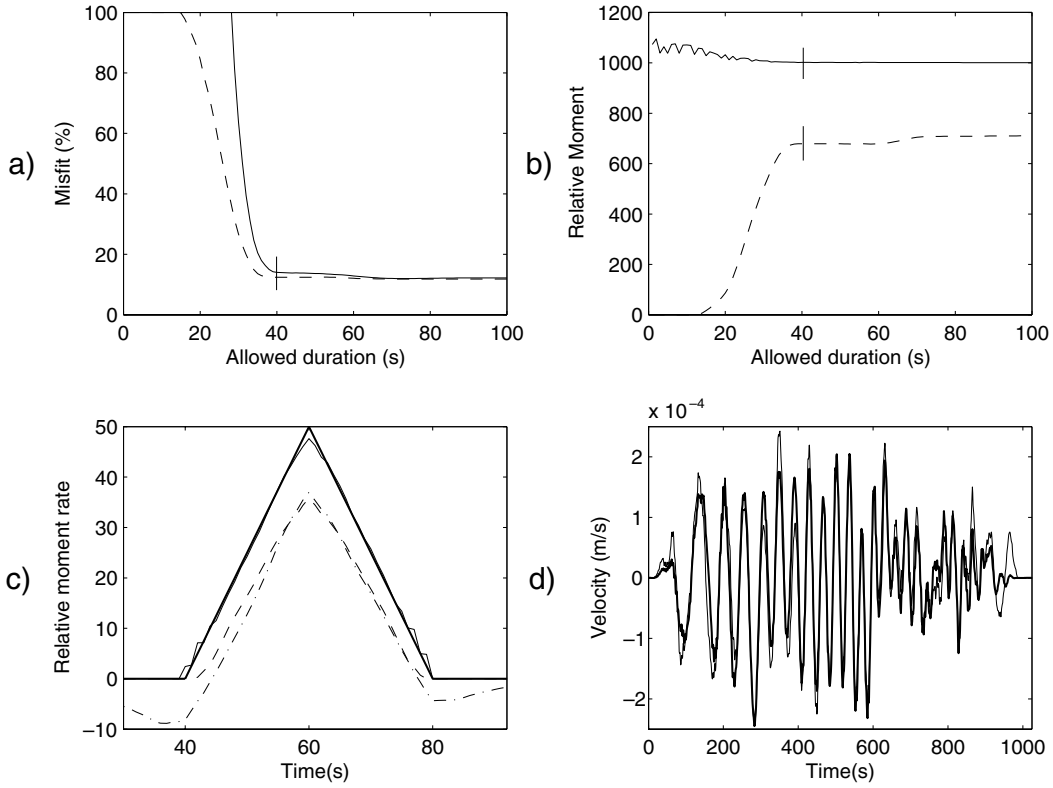

Figure 4. Results obtained, in the perpendicular direction, for the three deconvolution techniques considered in the synthetic case. Notations and panels as in Figure 3. For clarity, the scale in (c) is different from Figure 3c. In this direction, the reconstruction of RSTF with technique 1 is very close to the real RSTF.

We notice that the durations are correctly retrieved whatever technique is used but that the amplitudes are not reliable when we do not impose the moment. Our constrained moment deconvolution gives better results than the other techniques: reconstruction of the RSTFs is very good in the antidirective and perpendicular directions. Only in the directive direction, where the noise added to the EGF was high at low frequencies, is the moment release peak not completely retrieved.

Realistic Test with Differences in Location and Focal Mechanism: A Peru Synthetic Case

Our second synthetic example is even more realistic: we propose to compute synthetic mainshock waveforms by convolution between synthetic source time functions and a real EGF and then to use our deconvolution method with another EGF. This approach is close to the real case in which there are always some differences in focal mechanism and location between the EGF and the mainshock.

We use earthquakes that occurred close to the 23 June 2001 Peru earthquake, which will give an insight for the next section dedicated to this earthquake. We select two EGFs: the first one is an M_w 5.8 earthquake that occurred on 3 August 2000, and the second is an M_w 6.7 earthquake that occurred on 26 June 2001 (the same earthquake that we will use as the EGF in the next section). Both selected waveforms are presented in Figure 6. The locations and timings of these two events are retrieved from the International Seismological Center bulletin, which reveals a 40-km location difference between the hypocenters of the two events. According to the Harvard Centroid Moment Tensor (CMT), the 3 August 2000 and 26 June 2001 event mechanisms have strike, dip, and rake equal to 309°, 29°, and 66° and 314°, 19°, and 75°, respectively. We use the same three RSTFs as in the previous example and convolve them with the Love-wave field of the M_w 5.8 event. The resulting synthetic mainshocks are presented in Figures 7d, 8d, and 9d.

We now examine how well we are able to retrieve the initial RSTFs using the M_w 6.7 event as an EGF. We must take into account the nonzero duration of the chosen EGF. Because the source time function of this event is close to a 4-sec-long triangle (SOUM, 2001), we apply a 2-sec shift to the waveforms so that the source time function is now centered at the time 0 sec. We also apply a 80-sec high-pass filter to both EGF and mainshock waveforms to suppress the unreliable frequencies below the instrument low-pass cutoff. We then use the same three methods as before: the classical water-level approach, Bertero *et al.*'s (1997) approach, and our approach, in which the relative moment is constrained to the moment ratio between the mainshock and EGF. To

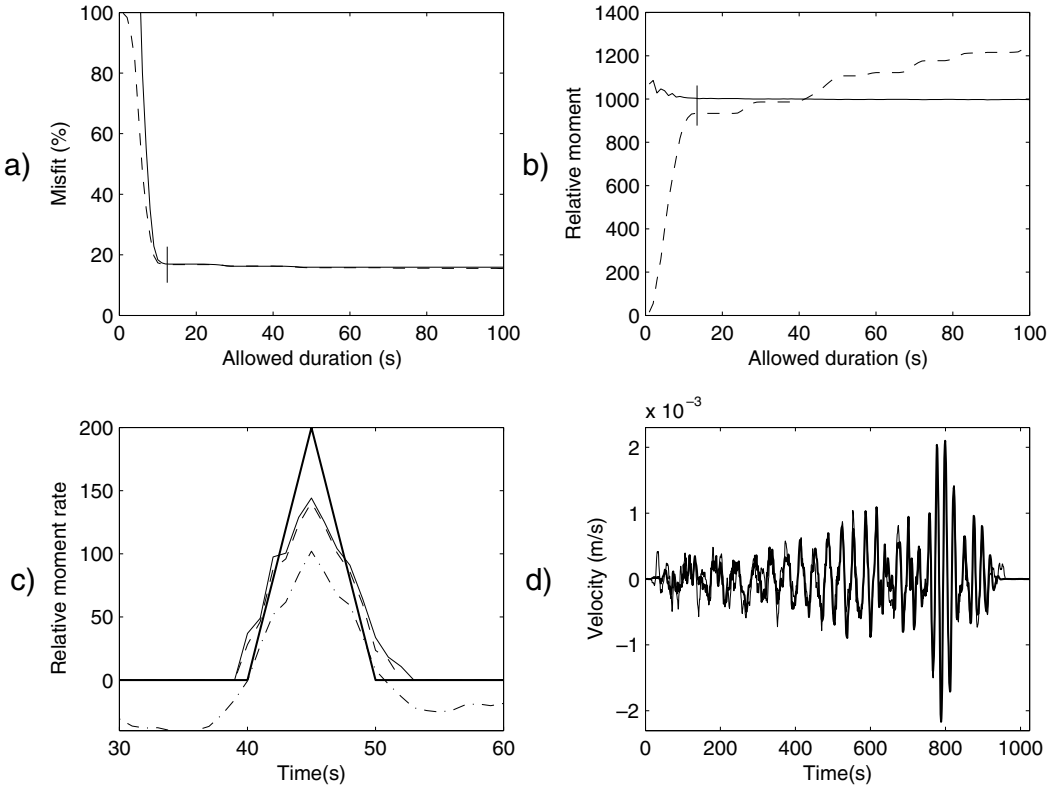

Figure 5. Results obtained, in the directive direction, for the three deconvolution techniques considered in the synthetic case. Notations and panels as in Figure 3. For clarity, the scale in (c) is different from Figure 3c. In this direction, all techniques underestimate the moment release peak of the real RSTF.

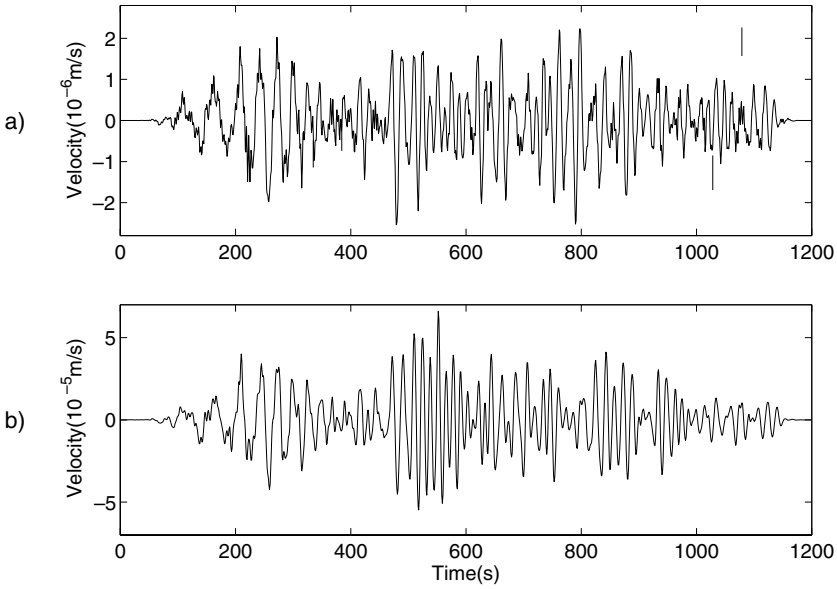

Figure 6. Love waves recorded at station FDF (Martinique, Carribean Sea) for two earthquakes occurring in the southeast Peru subduction zone: (a) an M_W 5.8 event occurring on 3 August 2000 and (b) an M_W 6.7 event occurring on 26 June 2001. The first waveform will then be convolved with synthetic source time functions to obtain synthetic mainshocks, whereas the second waveform will be used to estimate our ability to retrieve the synthetic source time functions.

determine this moment ratio, we use Harvard CMT inferred values. This implies that our synthetic mainshock has a moment equal to 6.55×10^{20} N m (taking into account the 1000 N m RSTF used to compute the mainshock) and the selected EGF a moment equal to 1.4×10^{19} N m, yielding a moment ratio equal to 46.7.

Results are presented in Figures 7, 8, and 9 in a similar manner to the first synthetic case. Figure 7 shows the antidirective direction. The water-level method can only be used to identify the apparent duration of the earthquake (70 sec). The large negative parts, as well as the erroneous amplitudes, would make a real inversion of the RSTFs very difficult. The

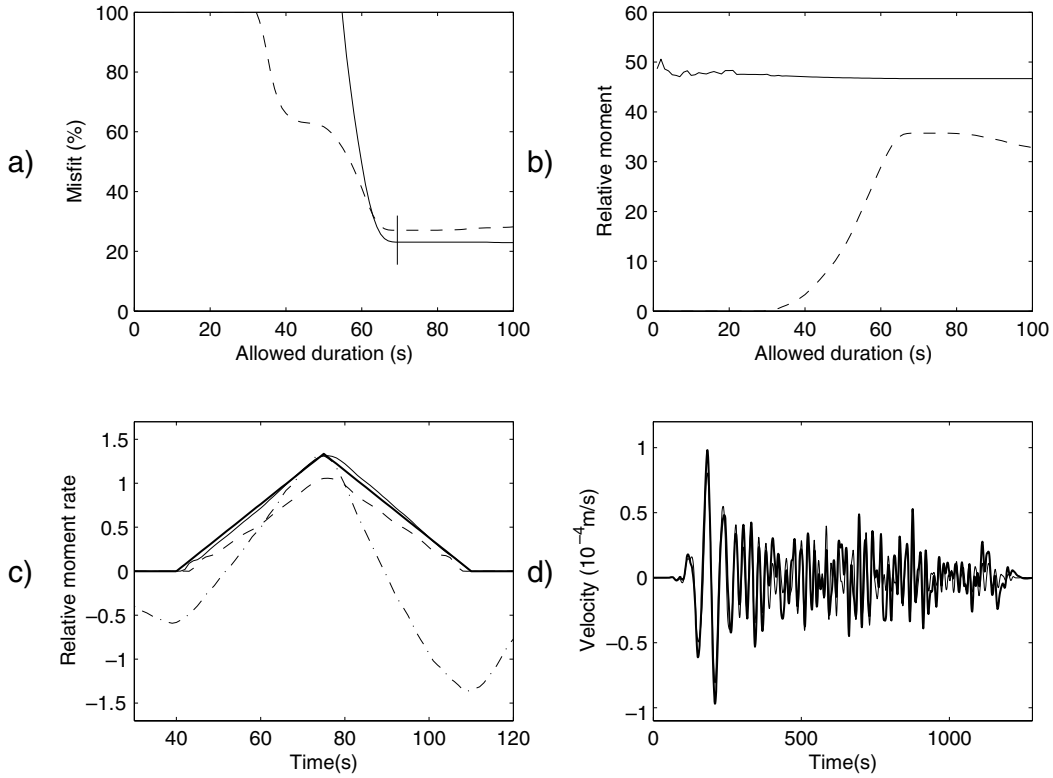

Figure 7. Results obtained in the antidirective direction for the Peru synthetic case, with the three deconvolution techniques. Notations and panels as in Figure 3. The constrained moment method gives a very good reconstruction of the source time function.

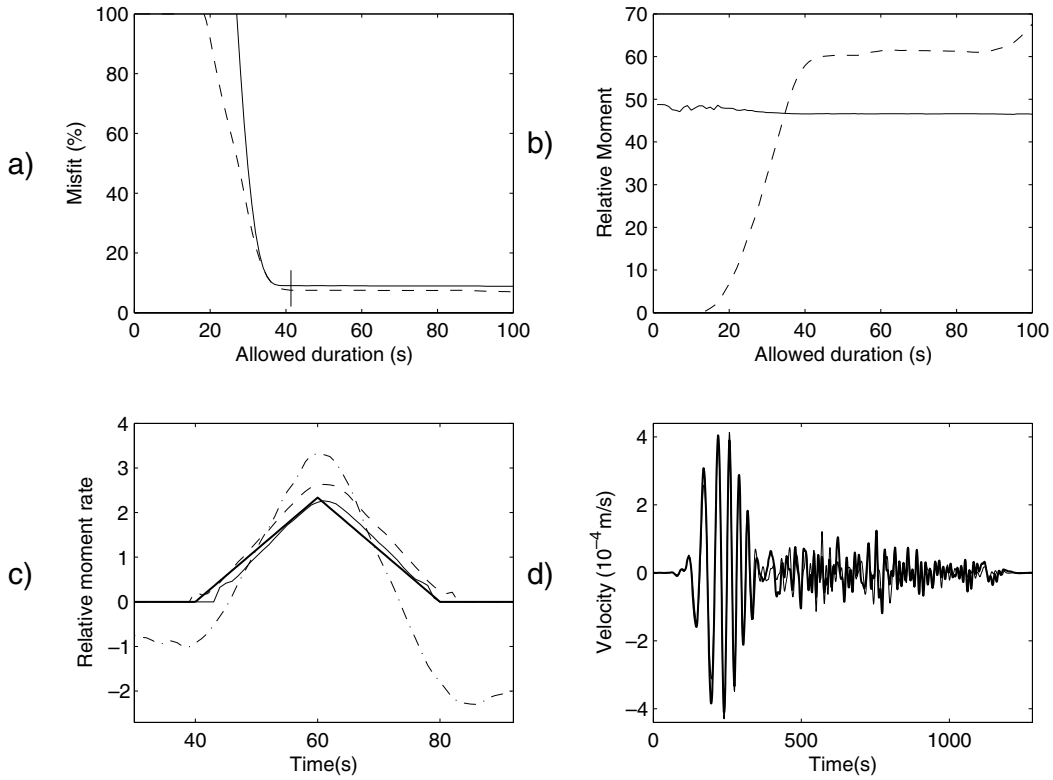

Figure 8. Results obtained in the perpendicular direction for the Peru synthetic case, with the three deconvolution techniques. Notations and panels as in Figure 3.

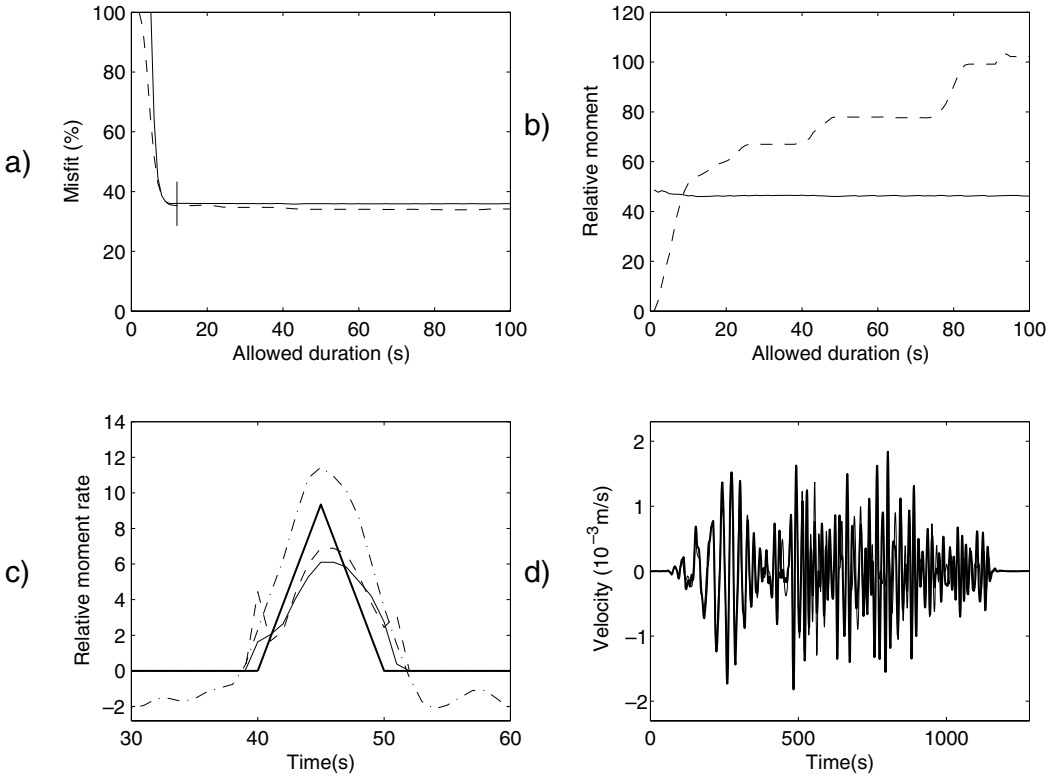

Figure 9. Results obtained in the directive direction for the Peru synthetic case, with the three deconvolution techniques. Notations and panels as in Figure 3. The quality of reconstruction is not as good as in the two other tests because the source time function has a much higher frequency content.

Bertero *et al.* (1997) method is more efficient, but the amplitudes are not well estimated. Our approach gives a RSTF very close to the real one. The obtained RSTF can therefore be used in an inversion of the earthquake rupture process. Similar conclusions can be drawn from the observation of Figure 8, which simulates the case of a rupture propagation observed in the perpendicular direction.

The directive case (Fig. 9) does not give results as reliable as before, even for the constrained moment method. This is mainly due to the fact that the frequencies considered are much higher than before (the RSTF is now 10-sec long). These high frequencies are more sensitive to the differences between the two selected earthquakes and are also closer to the corner frequency of the EGF.

These synthetic tests show that the constrained moment method is an efficient technique to retrieve the RSTFs. As could be predicted, the main limitation concerns the higher frequency content of the RSTFs (around and above 0.1 Hz). We now apply this technique to infer the source process of the Peru mainshock (23 June 2001, M_w 8.4) and to compare our results with other source studies of this event.

Application to the 23 June 2001 Peru Earthquake

The 23 June 2001 Peru earthquake (M_w 8.4) is the largest earthquake of the Harvard CMT catalog, that is, the largest earthquake since 1976. A complete report of the earthquake can be found in Tavera *et al.* (2002); they estimated the aftershock zone to be a rectangle of 160 km × 370 km (along trench), which is located almost completely southeast of the hypocenter. Three days after the earthquake, the M_w 6.7 aftershock that we used in the previous analysis occurred in the mainshock rupture zone. Its thrust focal mechanism is similar to the mainshock mechanism (which has a strike, dip, and rake equal to 310°, 18°, and 63° according to the Harvard CMT), and this event is therefore selected as an EGF of the mainshock. We use the method detailed in the previous sections to infer the main rupture properties of this major event. The along-trench rupture dimension is dominant in such a large subduction earthquake, and we therefore limit our study to a line source analysis along this direction.

Constrained RSTFs

According to the Harvard CMT, the mainshock moment is 4.67×10^{21} N m and the moment of the selected EGF is 1.4×10^{19} N m, yielding a ratio of 333. We will therefore constrain the RSTFs to respect this value in our deconvolution method. The deconvolutions are systematically tested with all stations of the IRIS-Geoscope networks, which recorded both events. We consider both Rayleigh-wave and Love-wave windows, but because of their higher quality, we finally select only RSTFs coming from Love waves. Since

we model the event as a line source, we choose to restrict our analysis to azimuths close to the fault strike; hence, we only consider stations that have an azimuth around 120° or around 300°. Stations at other azimuths are in fact more sensitive to along-dip details of the rupture, which are not modeled in a simple line source analysis. To be selected, RSTFs must respect the following criteria: (1) when reconvolved by the EGF, they yield a good fit to the real mainshock waveforms; and (2) the flat level of the misfit function (see, for example, Figs. 7a, 8a, and 9a) can be identified. With these criteria, we select two stations in the southeast direction (SHEL and SUR) and two stations in the northwest direction (KDAK and HDC). The EGF signals can be seen in Figure 10 and the Love-wave windows for the mainshock in Figures 11d,h and 12d,h.

We present in Figures 11 and 12, in a similar way as in previous figures, the results provided by our deconvolution method. Stations SHEL and SUR do not have a clear flat level of the misfit function (Fig. 11), but the use of longer and more complex RSTFs would have provided a fit improvement of at most 10%. Moreover, the examination of longer RSTFs shows that the dominant feature of the RSTFs, that is, a main pulse with 50-sec duration, remains constant. Stations KDAK and HDC have a clear flat level (Fig. 12), and the corresponding RSTF can therefore be easily identified.

To suppress the unreliable high frequencies of the RSTFs (Figs. 11 and 12), we do not use a low-pass filter, because it would affect both the positivity and the area of the RSTFs. We instead smooth the RSTFs with a cutoff frequency equal to 0.05 Hz. Velasco *et al.* (1994) have shown that for a rupture longer than about 100 km, frequencies higher than about 0.05 Hz are not reliable because of the finite duration of the EGF and the intrarupture surface wave dispersion. Figure 13 presents the smoothed RSTFs, which will now be used to infer the rupture process of the large Peru earthquake.

Interpretation in Terms of Line Source

The shape of the RSTFs confirms immediately that rupture propagated toward the southeast: the RSTFs are shorter and more impulsive at stations SUR and SHEL compared to stations KDAK and HDC. This is consistent with the aftershock zone of the earthquake or with the kinematic models of ERI (2001) and Sladen and Madariaga (2002). To retrieve more quantitatively the rupture properties of this earthquake, we model it as a line source. We have not investigated a two-dimensional source modeling (as defined by Olson and

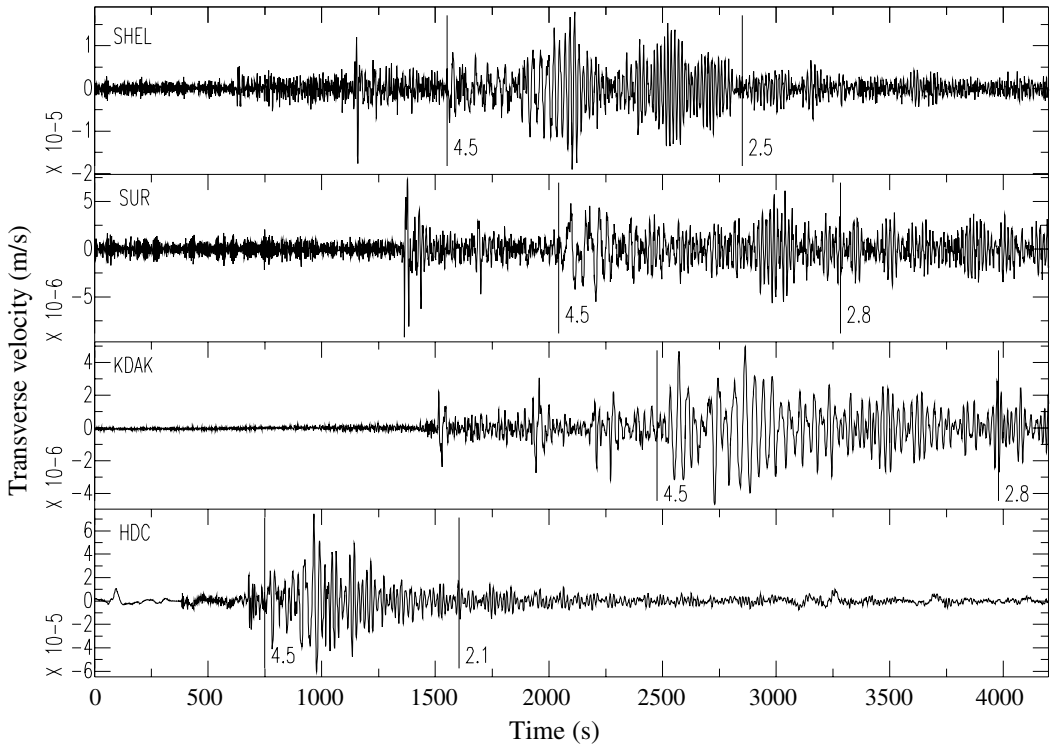

Figure 10. Transverse components of the EGF for the four stations used in the Peru earthquake analysis. The name of each station is indicated in the upper left-hand corner of each panel. The origin time is the origin time of the EGF (i.e., 26 June 2001, 04:18:32). The selected Love-wave window for each station is denoted by the two vertical bars, and the average horizontal velocities are given for the beginning and end of each window. The signals will be tapered later to zero at each extremity of the windows (and the selected waveforms will then be similar to these of Fig. 6).

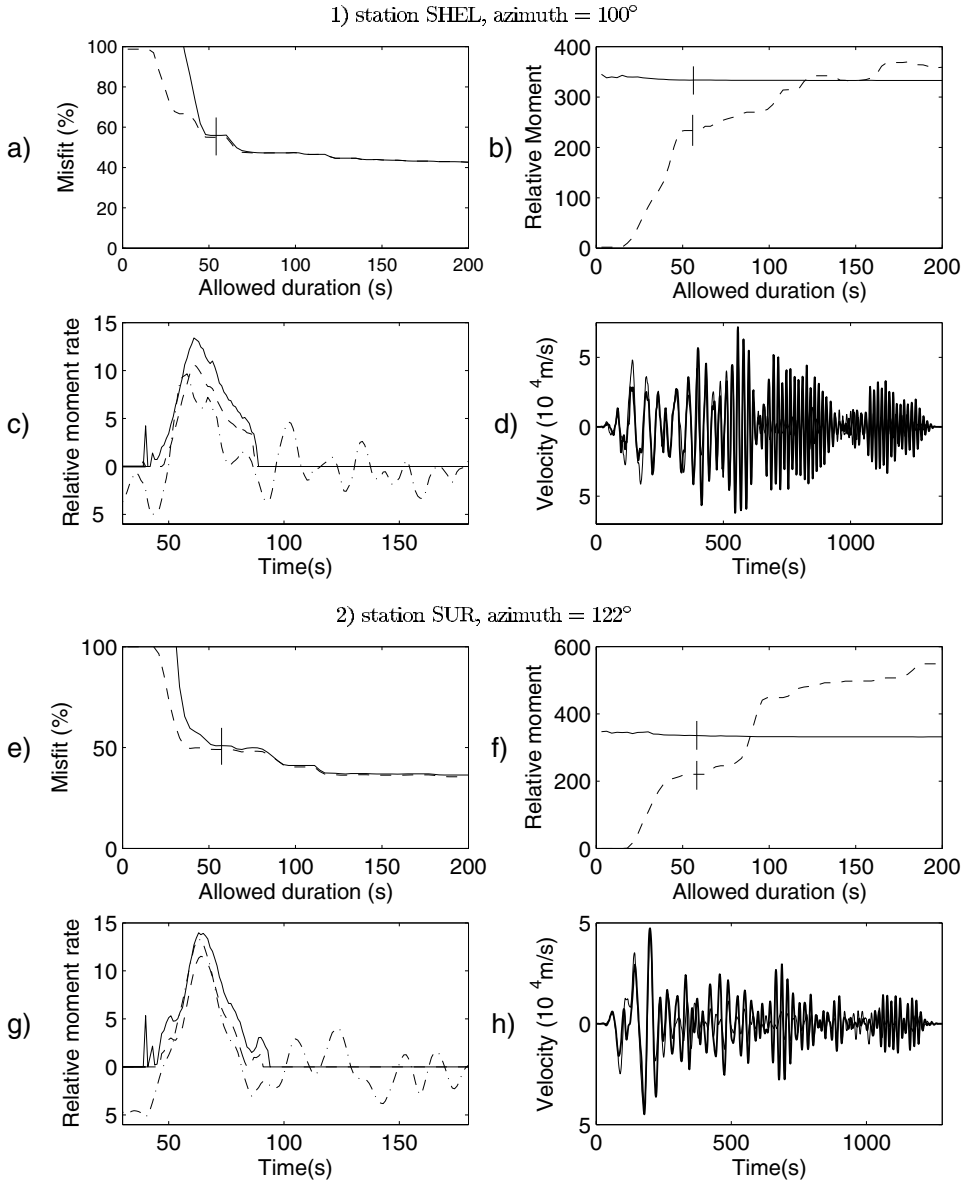

Figure 11. Results for the Peru earthquake, with the three deconvolution techniques. The two selected directive stations, SHEL and SUR, are represented with the same notations as in Figure 3. In both cases, we select a 60-sec global duration, because little improvement (around 10%) is gained by longer and more complex RSTFs. Note that the RSTF moments vary significantly when this constraint is not imposed (panels b and f). The high frequencies of the constrained RSTFs (panels c and g) are not reliable, because they are on the order of the corner frequency of the EGF (0.3–0.5 Hz). We will smooth them when fitting the RSTFs with a line source model (Fig. 13).

Apsel [1982] or Hartzell and Heaton [1983]) because the reliable frequencies of our analysis are too low to precisely image the along-dip propagation of the rupture. We determine after a few tests that the maximum rupture length L is 300 km, and we locate the hypocenter 60 km away from the northwestern end of the rupture. Observation of the antidirective RSTFs shows that they consist of two main features: a low-energy pulse during the first 80 sec and a larger pulse centered around 100 sec. We thus propose the following parametrization: the moment per unit width M_l is retrieved for each point of the line source, whereas the rupture velocity v_r and the duration of M_l, noted d, can only take two different values, one for each of the main pulses. We assume a triangular moment rate time function $Tr(M_l, d, t)$, so the synthetic RSTF $\tilde{F}_\theta$ for a given azimuth θ is defined by

$$\tilde{F}_\theta(t) = \int_0^L Tr\left(M_l(x),d(x),t - T(x) + \frac{x\cos(\theta - \theta_F)}{v_\phi}\right) dx, \quad (28)$$

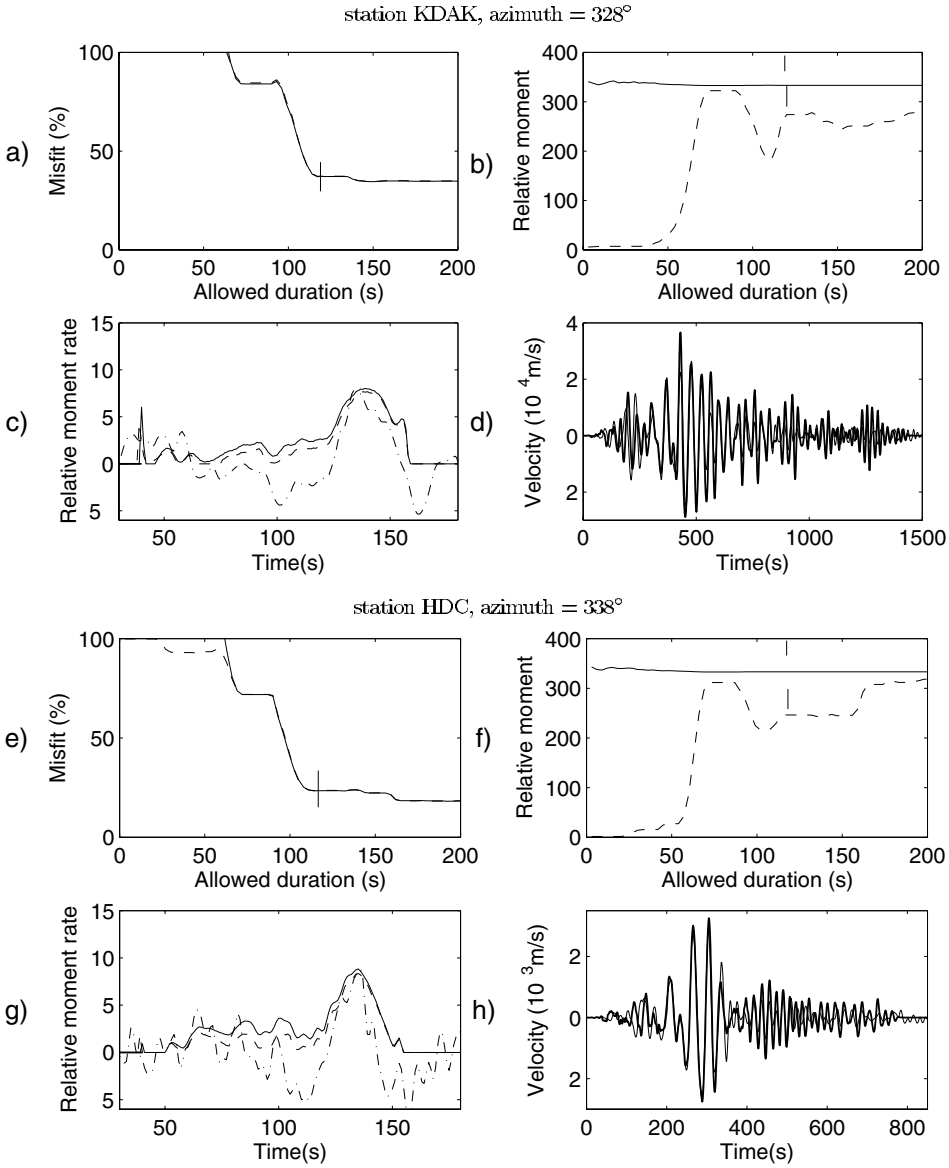

Figure 12. Results for the Peru earthquake, with the three deconvolution techniques. The two selected antidirective stations, KDAK and HDC, are shown with the same notations as in Figure 3. In both cases, we select a 120-sec global duration, because no improvement is obtained by a longer and more complex RSTF (panels a and e). The high frequencies of the constrained RSTF (panels c and g) are not reliable, because they are on the order of the corner frequency of the EGF (0.3–0.5 Hz). We will smooth them when fitting the RSTFs with a line-source model (Fig. 13).

where T is the onset time (depending on the rupture velocity model) and θ_F is the fault azimuth, approximated here at 122°. The phase velocity of Love waves v_ϕ is averaged to 4.4 km/sec (Ammon *et al.*, 1993). We discretize the fault in 30-km-long segments, so the synthetic RSTFs are described with 15 parameters (11 parameters for M_1 and 2 parameters for both d and v_r). v_r is constrained to be slower than the Rayleigh-wave velocity, which is here considered equal to 3.5 km/sec (but we checked that higher rupture velocities were not needed to explain the RSTFs). To find the optimal combination of the parameters, we minimize the relation

$$\text{Misfit} = \sum_{i=1}^{N} \int_0^D |\tilde{F}_{\theta i}(t) - F_{\theta i}(t)| dt, \qquad (29)$$

where N is the number of stations and D the maximum duration of the RSTFs. This inverse problem is solved by the neighborhood algorithm (NA) proposed by Sambridge (1999). We do not develop here the principles of this method. Details are fully explained in Sambridge's article, and applications to source studies can be found in Marson-Pidgeon *et al.* (2000) or Vallée *et al.* (2003).

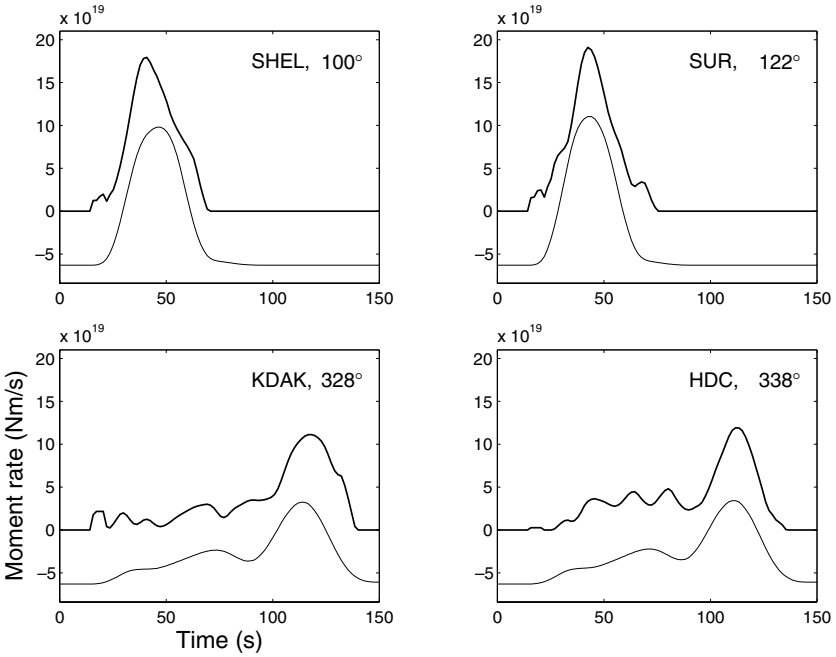

Figure 13. Selected RSTFs for the 23 June 2001 Peru earthquake. The thick lines are the real RSTFs, obtained by our constrained deconvolution. The thin lines are the synthetics related to the line source analysis of the mainshock (Fig. 14). Names and azimuths of the stations are specified inside each subfigure. Both data and synthetics have been smoothed with a cutoff frequency equal to 20 sec.

We show in Figure 13 the comparison between synthetic and observed RSTFs and in Figure 14 the source models found by the inversion. We present models obtained for M_l and v_r as well as the absolute source time function. We only present the average value of the rupture velocity because its values on each subfault are not well resolved, partly due to the well-known trade-off with duration d. Consequently, the duration d is not well resolved either (Ihmlé, 1998). As in Vallée *et al.* (2003), the standard errors on the parameters are evaluated by the use of a number of independent runs of the NA. The principle moment release zone is located 150 km away from the hypocenter. This is consistent with the kinematic model defined by ERI (2001); however, our resolution of the rupture extension is better than that derived from the body waves used in the latter model. This is because the slow phase velocity of the surface waves, as well as their horizontal propagation direction, is more efficient for imaging the lateral extension of the source.

If we assume a fault width of 120 km and a rigidity of 4.8×10^{10} N m^{-2} ($V_s \simeq 4$ km/sec and $\rho \simeq 3000$ kg/m^3 at 30 km depth), the slip approaches about 15 m on the high moment release portion of the fault. This is significantly higher than the maximum slip determined by ERI (8 m). However, the use of body waves alone is known to underestimate the global moment (Ekström, 1989). The total rupture lasted about 90 sec, and the mean rupture velocity is estimated to 2.9 km/sec. This application to this very large earthquake confirms the usefulness of our constrained method for imaging the large features of the source process.

Discussion and Conclusions

In this article, we have proposed a new method for stabilizing the EGF technique. Classically, EGF analysis is more reliable when used to identify the RSTF durations at various azimuths from the source. This gives an estimate of the length and mean rupture velocity of the event but brings little information about the locations and sizes of the main moment release zones. Moreover, the determination of these durations often depends on the interpretation of the author: when the end of the rupture is poorly defined, or when the RSTFs have a large negative part, different choices are possible. It would be more robust to rely on a global fit of the shape of the RSTFs, but this requires that they have sufficiently high quality.

We show here that the quality of the RSTFs is greatly improved if we take into account various physical constraints. The usefulness of the positivity, causality, and bounded duration constraints has already been shown by Bertero *et al.* (1997). In this study, we demonstrate that another physical constraint is particularly important: the area of the RSTFs, which is equal to the moment ratio between the mainshock and EGF, must remain the same at all stations. Moreover, this constraint can easily be included in the same projected Landweber algorithm as the one introduced by Bertero *et al.* (1997).

Examples in synthetic and semireal cases show that the RSTFs are more reliable when we use the equal moment constraint defined in this study. Thus, in the case of real

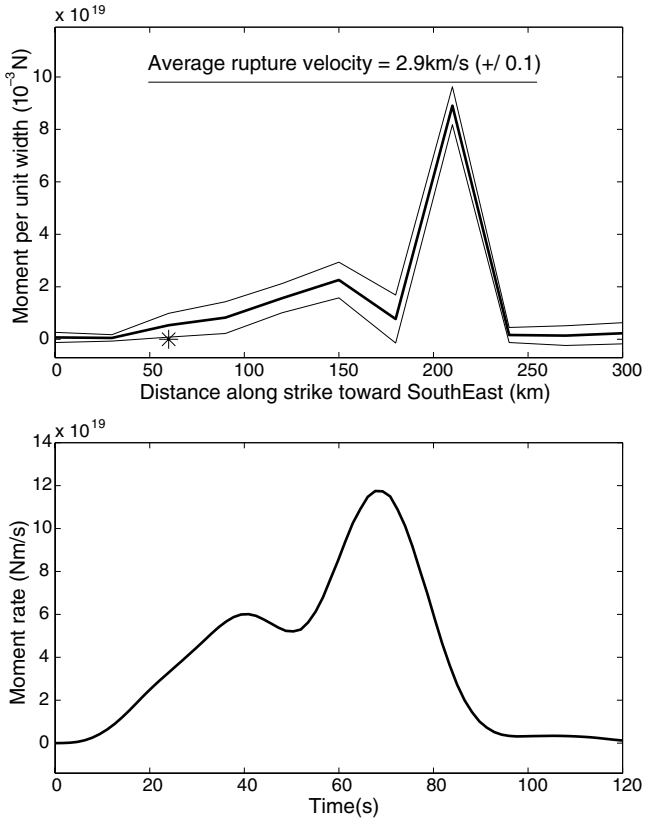

Figure 14. Line source modeling of the mainshock. Top Line source model for the moment per unit width. The thick line is the mean model of 10 independent runs of the NA. The two thin lines represent the extremal models (mean model ± 3 times the standard error). The hypocenter is denoted by a star. We have also represented the inferred mean value for the average rupture velocity, as well as its uncertainty (defined as 3 times the standard error). Bottom Absolute source time function corresponding to the the mean line source model presented in (a).

source analysis, we can directly infer the rupture properties by a fit of the RSTF waveforms. Our modeling of the large 23 June 2001 Peru earthquake reveals that its rupture propagated toward the southeast at about 2.9 km/sec and lasted about 90 sec. The inferred rupture length is about 180 km, and a zone of high moment release is well identified 150 km away from the hypocenter.

Acknowledgments

I am grateful to Michel Bouchon for his suggestions and comments. I thank Malcolm Sambridge, for providing me with the neighborhood algorithm code, and the IRIS and GEOSCOPE networks, from which I retrieved the worldwide recordings of the Peru earthquake. I thank Olivier Sèbe and Jocelyn Guilbert for helpful discussions. Jean Virieux and an anonymous reviewer contributed greatly to improve this article. This work was supported by a grant from the Centre National de la Recherche Scientifique (CNRS) and from the Commissariat a l'Energie Atomique (CEA/DASE).

References

Aki, K., and P. Richards (1980). *Quantitative Seismology: Theory and Methods*, W. H. Freeman, New York.

Ammon, C. J., A. A. Velasco, and T. Lay (1993). Rapid estimation of rupture directivity: application to the 1992 Landers ($M_S = 7.4$) and Cape Mendocino ($M_S = 7.2$), California earthquakes, *Geophys. Res. Lett.* **20,** 97–100.

Bertero, M. (1989). Linear inverse and ill-posed problems, in *Advances in Electronics and Electron Physics*, Vol. 75, P. W. Hawkes (Editor), Academic, New York, 1–120.

Bertero, M., P. Boccacci, and F. Maggio (1995). Regularization methods in image restoration: an application to HST images, *Int. J. Imaging Systems Tech.* **6,** 376–386.

Bertero, M., D. Bindi, P. Boccacci, M. Cattaneo, C. Eva, and V. Lanza (1997). Application of the projected Landweber method to the estimation of the source time function in seismology, *Inverse Problems* **13,** 465–486.

Centroid Moment Tensor (CMT) Catalog, www.seismology.harvard.edu/CMTsearch.html (last accessed February 2004).

Courboulex, F., M. A. Santoyo, J. F. Pacheco, and S. K. Singh (1997a). The 14 September 1995 (*M* 7.3) Copala, Mexico, earthquake: a source study using teleseismic, regional, and local data, *Bull. Seism. Soc. Am.* **87,** 999–1010.

Courboulex, F., S. K. Singh, J. F. Pacheco, and C. J. Ammon (1997b). The 1995 Colima–Jalisco, Mexico, earthquake (M_W 8): a study of the rupture process, *Geophys. Res. Lett.* **24,** 1019–1022.

Ekström, G. (1989). A very broad band inversion method for the recovery of earthquake source parameters, *Tectonophysics* **166,** 73–100.

Earthquake Research Institute (ERI) (2001). EIC seismological note: Peru Earthquake on June 23, 2001, University of Tokyo.

Fukuyama, E., and K. Irikura (1986). Rupture process of the 1983 Japan Sea (Akita-Oki) earthquake using a waveform inversion method, *Bull. Seism. Soc. Am.* **76,** 1623–1640.

Hartzell, S. H. (1978). Earthquake aftershocks as Green's functions, *Geophys. Res. Lett.* **5,** 1–4.

Hartzell, S. H., and T. H. Heaton (1983). Inversion of strong ground motion and teleseismic waveform data for the fault rupture history of the 1979 Imperial Valley, California, earthquake, *Bull. Seism. Soc. Am.* **73,** 1553–1583.

Ihmlé, P. F. (1996). Frequency-dependent relocation of the 1992 Nicaragua slow earthquake: an empirical Green's function approach, *Geophys. J. Int.* **127,** 75–85.

Ihmlé, P. F. (1998). On the interpretation of subevents in teleseismic waveforms: the 1994 Bolivia deep earthquake revisited, *J. Geophys. Res.* **103,** 17,919–17,932.

Ihmlé, P. F., and J. C. Ruegg (1997). Source tomography by simulated annealing using broad-band surface waves and geodetic data: application to the $M_w = 8.1$ Chile 1995 event, *Geophys. J. Int.* **131,** 146–158.

Kikuchi, M., and H. Kanamori (1982). Inversion of complex body waves, *Bull. Seism. Soc. Am.* **72,** 491–506.

Lawson, C., and R. Hanson (1974). *Solving Least Square Problems*, Prentice Hall, New York.

Marson-Pidgeon, K., B. L. N. Kennett, and M. Sambridge (2000). Source depth and mechanism inversion at teleseismic distances using a neighborhood algorithm, *Bull. Seism. Soc. Am.* **90,** 1369–1383.

Mori, J., and A. Frankel (1990). Source parameters for small events associated with the 1986 North Palm Springs, California, earthquake determined using empirical Green functions, *Bull. Seism. Soc. Am.* **80,** 278–295.

Mueller, C. S. (1985). Source pulse enhancement by deconvolution of an empirical Green's function, *Geophys. Res. Lett.* **12,** 33–36.

Olson, A. H., and R. J. Apsel (1982). Finite fault and inverse theory with applications to the 1979 Imperial Valley earthquake, *Bull. Seism. Soc. Am.* **72,** 1969–2001.

Piana, M., and M. Bertero (1997). Projected Landweber method and preconditioning, *Inverse Problems* **13,** 441–463.

Sambridge, M. (1999). Geophysical inversion with a neighbourhood algorithm. I. Searching a parameter space, *Geophys. J. Int.* **138,** 479–494.

Schwartz, S. Y. (1999). Noncharacteristic behavior and complex recurrence of large subduction zone earthquakes, *J. Geophys. Res.* **104,** 23,111–23,125.

Sladen, A., and R. Madariaga (2002). Nonlinear inversion of body waveforms of the June 2001 earthquakes in southern Peru, *EOS* **83** (Fall Meet. Suppl.), Abstract S71C-1105.

Tavera, H., E. Buforn, I. Bernal, Y. Antayhua, and L. Vilacapoma (2002). The Arequipa (Peru) earthquake of June 23, 2001, *J. Seismology* **6,** 279–283.

Seismological Observatory, University of Michigan (SOUM) (2001). www.geo.lsa.umich.edu/SeismoObs/STF/010626_Peru (last accessed February 2004).

Vallée, M., M. Bouchon, and S. Y. Schwartz (2003). The January 13, 2001 El Salvador earthquake: a multi-data analysis, *J. Geophys. Res.* **108,** no. B4, 2203, doi 10.1029/2002JB001922.

Velasco, A. A., C. J. Ammon, and T. Lay (1994). Empirical Green function deconvolution of broadband surface waves: rupture directivity of the 1992 Landers, California (M_W = 7.3), *Bull. Seism. Soc. Am.* **84,** 735–750.

Velasco, A. A., C. J. Ammon, and S. L. Beck (2000). Broadband source modeling of the November 8, 1997, Tibet (M_w = 7.5) earthquake and its tectonic implications, *J. Geophys. Res.* **105,** 28,065–28,080.

Youla, D. C., and H. Webb (1982). Image restoration by the method of convex projections. I. Theory, *IEEE Trans. Medical Imaging* **MI-1,** 81–94.

Laboratoire de Géophysique Interne et Tectonophysique
Observatoire de Grenoble, Université Joseph Fourier
BP 53, 38041 Grenoble Cedex 9
France

Manuscript received 16 January 2003.